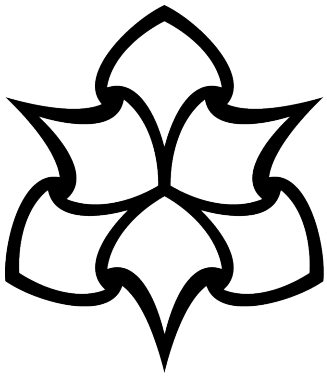

ADVANCED ENERGY MATERIALS
www.advenergymat.de

Next-Generation Additive Manufacturing of Complete Standalone Sodium-Ion Energy Storage Architectures

*Michael P. Down, Emiliano Martínez-Periñán, Christopher W. Foster, Encarnación Lorenzo, G. C. Smith, and Craig E. Banks**

The first entirely AM/3D-printed sodium-ion (full-cell) battery is reported herein, presenting a paradigm shift in the design and prototyping of energy-storage architectures. AM/3D-printing compatible composite materials are developed for the first time, integrating the active materials $NaMnO_2$ and TiO_2 within a porous supporting material, before being AM/3D-printed into a proof-of-concept model based upon the basic geometry of commercially existing AA battery designs. The freestanding and completely AM/3D-fabricated device demonstrates a respectable performance of 84.3 mAh g^{-1} with a current density of 8.43 mA g^{-1}; note that the structure is typically comprised of 80% thermoplastic, but yet, still works and functions as an energy-storage platform. The AM/3D-fabricated device is critically benchmarked against a battery developed using the same active materials, but fabricated via a traditional manufacturing method utilizing an ink-based/doctor-bladed methodology, which is found to exhibit a specific capacity of 98.9 mAh m^{-2} (116.35 mAh g^{-1}). The fabrication of fully AM/3D-printed energy-storage architectures compares favorably with traditional approaches, with the former providing a new direction in battery manufacturing. This work represents a paradigm shift in the technological and design considerations in battery and energy-storage architectures.

1. Introduction

The utilization of rechargeable sodium-ion batteries (SIBs) is regarded as the most favorable renewable energy storage system due to the low cost and abundance of sodium.[1–4] A number of recent studies on sodium intercalation compounds have focused upon Earth abundant and hence low cost transition metals, especially Mn and Fe, which would allow for economical prototyping of energy storage concepts. Potential sodium intercalation cathodes, such as 3D framework compounds, especially those based on the NASICON structure, have received considerable attention because of high Na^+ conductivity.[5–9] Where layered Li transition metal oxides such as $LiCoO_2$ and related materials have been dominant cathodes for lithium-ion cells,[10,11] layered Na transition metal compounds, namely $NaMnO_2$, exhibit extensive intercalation chemistry, more so than their Li counterparts. For example, both $NaFeO_2$ and $NaCrO_2$ are electrochemically active compared to their lithium analogs and $NaMnO_2$ compounds can sustain sodium deintercalation without conversion to the spinel structure, unlike layered $LiMnO_2$. Typically, within the literature, these SIBs are manufactured via simple 2D-printing process, such as screen-printing and doctor-blading, offering an effective platform for the benchmarking and testing of an array of anode and cathode materials, but demonstrating a low geometrical surface area and/or electrode/electrolyte interaction. However, recently researchers have started to shift toward additive manufacturing (AM)/3D printing for the design of fabrication of advanced functional materials and novel frameworks, for the prototyping of energy storage devices.[12,13]

Many of the current AM/3D energy storage systems developed within the literature utilize a direct-write technology, where the print is formed of a fluidic compound, printed layer-by-layer, before requiring curing, by either heat, UV exposure or nitrogen freezing. This "curing/freezing" is required to solidify the printed model, resulting in a system that is highly restricted in the vertical *z*-direction, and experience significant warping and shrinkage.[13,14] Within the AM/3D printing community, extrusion-based AM/3D printing (fused deposition

Dr. M. P. Down, Dr. E. Martínez-Periñán, Dr. C. W. Foster, Prof. C. E. Banks
Faculty of Science and Engineering
Manchester Metropolitan University
Chester Street, Manchester M15 GD, UK
E-mail: c.banks@mmu.ac.uk
Dr. M. P. Down, Dr. C. W. Foster, Prof. C. E. Banks
Manchester Fuel Cell Innovation Centre
Manchester Metropolitan University
Chester Street, Manchester M1 5GD, UK
Dr. E. Martínez-Periñán, Prof. E. Lorenzo
Departamento de Química Analítica y Análisis Instrumental
Universidad Autónoma de Madrid
28049, Madrid, Spain
Prof. G. C. Smith
Faculty of Science and Engineering
Department of Natural Sciences
University of Chester
Thornton Science Park, Pool Lane, Ince, Chester CH2 4NU, UK
The ORCID identification number(s) for the author(s) of this article can be found under https://doi.org/10.1002/aenm.201803019.

DOI: 10.1002/aenm.201803019

modeling, FDM), in which a uniform filament of thermoplastic polymer is heated past its softening point and extruded and cured (in situ) into layers defined by the models geometry,[15,16] is the most universal owing to its straightforward printing principle and inexpensive manufacturing process.[17] Recently however, research into FDM printable filaments has been minimal and the introduction of a high loading of nanomaterials within a thermoplastic support is limited, with current commercial filaments offering little applicability within the field of energy storage.[18,19] Therefore, the manufacture and fabrication of highly active 3D printable filaments are paramount to the success of AM/3D printed energy storage devices.

Foster et al. have demonstrated that the use of commercially available electrically conducting filaments can be applied as freestanding anodes within lithium-ion batteries.[18] In their study, a solid commercially available filament was utilized to demonstrate the potential of additive manufacturing as an experimental approach to development of energy storage architectures. This study looks to build upon the proven principle demonstrated by Foster et al. and reports the integration of not only sodium active materials but also porous microstructures into AM filaments. Consequently, this paper reports the first freestanding sodium-ion (full cell) battery formed entirely of components that have been fabricated via AM/3D printing. This approach is a novel and contemporary solution for the development of the next generation of energy storage systems integrating the active materials $NaMnO_2$ and TiO_2 within a highly novel porous supporting material, designed to maximize electrode surface area, before being AM/3D printed into a proof-of-concept model based upon the basic geometry of a commercially available AA battery (see **Figure 1**).

Structural and Physical Characterization of $NaMnO_2$: This paper reports the first sodium-ion (full cell) battery formed entirely of components that have been fabricated via AM/3D printing (described within the Experimental Section and overviewed within Figure 1) and are critically compared to the traditional printing/doctor blading commonly within the literature.

NMR (^{23}Na) was utilized in order to confirm the composition and conformity of the $NaMnO_2$ sample fabricated herein. **Figure 2** shows the NMR spectra, which exhibits stacking akin to that of nominally pure β-$NaMnO_2$ samples.[20–23] The ^{23}Na NMR of the $NaMnO_2$ sample at both 4.7 and 8.4 T show two isotropic resonances, indicating two distinct sodium environments. The isotropic resonance is primarily due to the $1/2 \leftrightarrow -1/2$ transition, which is only affected to second order by quadropolar interactions. The spinning sidebands present, which are highlighted by the green bars, are primarily due to the $\pm 3/2 \leftrightarrow \pm 1/2$, which is only affected to second order by the quadropolar interaction; the peaks located at roughly 438 and 240 agree closely with those reported in the academic literature.

To understand the structural characteristics of the $NaMnO_2$ that allow for the sodium deintercalation and reinsertion, the structure of the $NaMnO_2$ was analyzed by powder X-ray diffraction, and solid-state NMR. The X-ray diffraction (XRD) pattern of the as-prepared monoclinic $NaMnO_2$ is shown in Figure 2. Through utilizing a Reitveld refinement of the crystalline structure, the lattice parameters are defined as, a = 5.649 Å, b = 2.829 Å, c = 5.769 Å, β = 112.8°. These values are closely related to those found in literature (a = 5.63 *Å*, b = 2.86 *Å*, c = 5.77 *Å*, β = 112.9°).[24,25] Given this and the crystalline structure of $NaMnO_2$, the Mn—O bond lengths in the MnO_6 octahedron are 2.30 Å (2×) and 1.84 Å (4×) respectively. This analyses confirms the activity of the $NaMnO_2$ according to the Jahn–Teller effect.[23] Further to this, the DCP data, assuming that the prepared materials are completely phase pure, the chemical formula is determined to be $NaMnO_{2.09}$.

It is apparent from Figure 2A that the structure of $NaMnO_2$ is not ideally structured, in that it does not represent a $NaMnO_2$ sample and features both crystalline formations of $NaMnO_2$,

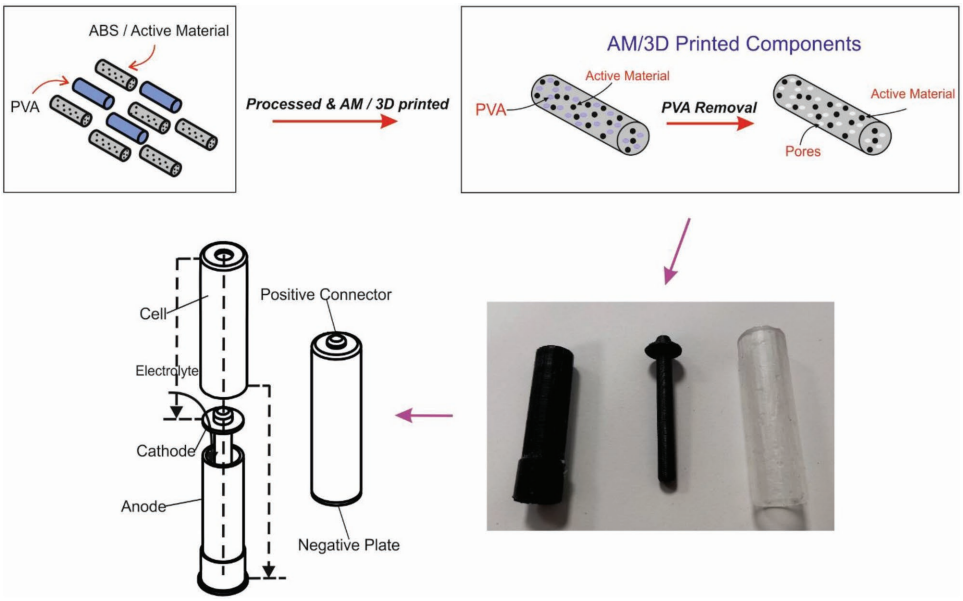

Figure 1. Schematic illustration and photographs of the fabrication procedure of the complete freestanding fully AM/3D printed sodium-ion battery.

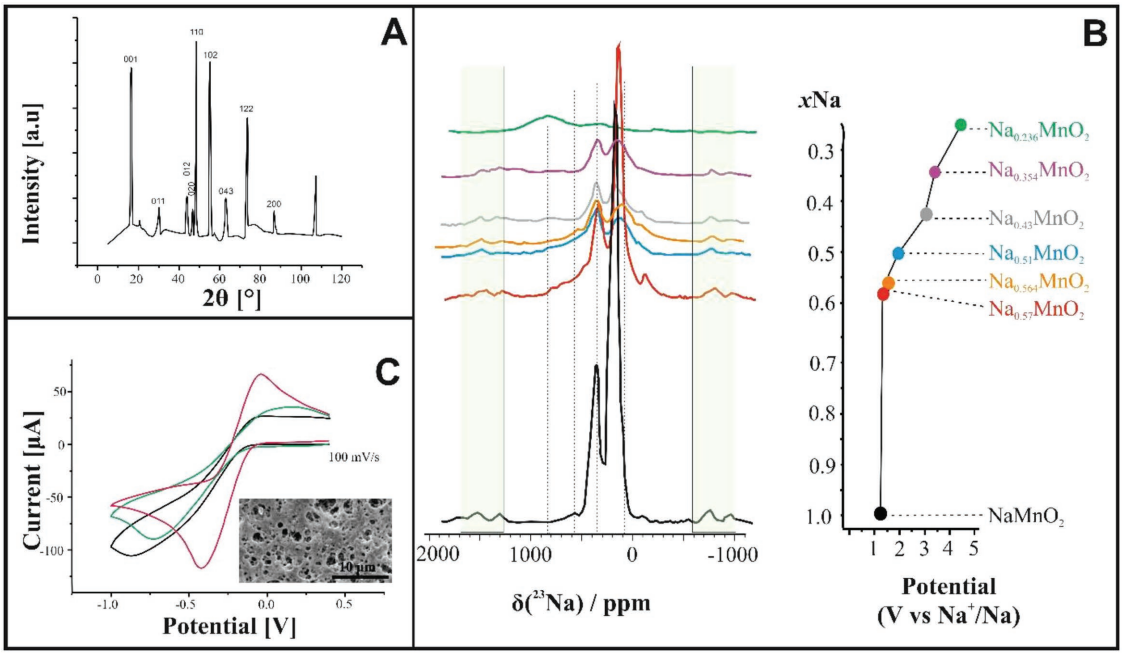

Figure 2. The physicochemical and chemical characterization of the various AM/3D printed energy storage architectures. A) XRD of the $NaMnO_2$ integrated into the AM/3D printed energy storage architectures (electrodes); B) Ex situ 23Na spin echo NMR spectra obtained under an external field of 200 MHz and ay a spinning frequency of 60 kHz. The green bars identify sidebands. The test conditions were to replicate those carried out by Billaud et al. to ensure the relative quality of the $NaMnO_2$ of this sample used;[20] C) Cyclic voltammograms of the compositional variation of AM/3D printed polymer-based energy storage architectures (electrodes) which comprise: 80% PVA/ABS [1:1]/20% Super P nanocarbon and 80% PVA/ABS [1:1]/20% Super P nanocarbon following sonication in deionized water for 4 h to remove the PVA (red), and 80% ABS/20% PVA as a benchmark (green)—all in 0.5 M $NaBF_4$ within $EMIBF_4$. Shown in the inset of 2 C is an SEM image of the 80% PVA/ABS [1:1]/20% Super P following sonication in deionized water for 4 h.

α-$NaMnO_2$ (indicated largely by the presence of the (011) peak) and β-$NaMnO_2$ (this is the specific crystalline arrangement of $NaMnO_2$ that contributes to the Jahn–Teller activity).[20,21,25] The crystalline faults observed here are indicative of a specific form of MnO_2, largely referred to as Ramsdellite. Such crystalline faults are uncommon in battery materials.[20,21,25] The stacking faults in the $NaMnO_2$ structure can in fact be closely related to those in the isostructural $LiMnO_2$ material, and even the Jahn–Teller distorted $LiMnO_2$.[24,26] Despite these faults, there is significant correlation between this crystalline structure and those found in the literature.[21,23] The crystalline structure even compares to the cases where the structure is claimed to be purely β-$NaMnO_2$ despite proportions of stacking faults up to those of up to 25%.[20–22]

Figure S1 (Supporting Information) shows the HRTEM and SAED characterization of the $NaMnO_2$ prior to integration into the 3D printing polymer matrix. The analysis indicates a number of planes present, confirming the representative analysis of the XRD. Additionally, SEM analysis is presented in Figure S2 (Supporting Information), where it is clear that the $NaMnO_2$ crystals have been formed. X-ray photoelectron spectroscopy (XPS) is presented in Figure S3 (Supporting Information), exhibiting the compositional spectral analysis of the material. The survey spectrum demonstrates strong Na, Mn, and O peaks, as expected. The peak at ≈495 eV is the X-ray excited Na KVV Auger peak, with weaker components of this series also present in the spectrum. One of these components overlaps with the O 1s signal (see below). The Mn also shows a series of X-ray excited Auger peaks in the range 700–900 eV. The peak ≈950 eV is a further X-ray excited peak, O KVV. Weak peaks were also seen due to C, Zr, and Al. The Al is associated with a low level of signal from the surround of the sample holder. Its binding energy from the survey spectrum was ≈181.5 eV, consistent with ZrO_2. The slight presence of ZrO_2 (<<1%) is a likely consequence of the ball milling processing during the synthesis of the active material. A contribution to the C 1s signal is from the low level of atmospheric hydrocarbon contamination present on the surface; a further contribution is believed to be associated with the "true" composition of the sample.

Freestanding Fully AM/3D Printed (Full Cell) Na-Ion Battery: The energy storage architecture is developed entirely using AM/3D printed components. In order to do this, the active battery materials have to be integrated into a porous polymer matrix; without this, the electrolyte cannot penetrate the active components and the lack of a triple-phase boundary means that an AM/3D printed structure without porosity, is a poor/completely useless battery. Therefore, a porous polymer matrix was developed by integrating an immiscible water-soluble polymer into an AM/3D printable polymer matrix. In this case, PVA is mixed into an ABS polymer matrix along with the active materials, $NaMnO_2$ for the cathode, and a TiO_2 nanopowder for the anode, along with the inclusion of Super P nanocarbon in order to enhance the electrochemical conductivity. The resulting composites are extruded into AM/3D printable filaments and manufactured via FDM AM/3D printing an

appropriate electrode design/energy storage architectures. The AM/3D printed electrodes are then sonicated in water for 4 h to remove the micropockets of PVA (as PVA is easily dissolvable within water), leaving microporous electrochemically active AM/3D printed electrodes/energy storage architectures. The resulting electrode/structure is dried at 60 °C and stored under vacuum; this overall process is summarized within Figure 1.

The resulting cells were tested with cyclic voltammetry within an ionic liquid with the cycling stability explored at cycles of 1, 100, 500, and 1000. Figure S4 (Supporting Information) shows the resultant cyclic voltammograms, which indicates a high level of potential cycling of the cell. A significant peak is apparent for each of these cycles at about +0.8 V indicating the deintercalation of the cathodic, and anodic insertion of the sodium cations. The decrease in the peak current, with cycling, can potentially be attributed to the lack of mobility of sodium ions in graphitic structures and the embedding of the ions in the anode, reducing the efficiency of the device. During this period, there was little structural or physical change to the cell exterior indicating a significant and robust AM/3D printed cell.

Bespoke AM/3D filaments are developed for the first time: 80% PVA/ABS [1:1]/20% Super P nanocarbon and 80% PVA/ABS [1:1]/20% Super P nanocarbon and 80% ABS/20% PVA as a benchmark. The 80% ABS/PVA [1:1] 20% Super P was used without soaking or sonicating in water, while the 80% ABS/PVA [1:1] and 20% Super P was sonicating in water (4 h); the sonication acts as to remove the micropockets of PVA, introducing pores into the AM/3D printed structure/electrode architecture which results in a structure with microporosity and hence a significantly increased surface area, as shown within inset of Figure 2C.

AM/3D printed electrodes of 3 mm diameter, as described by Foster et al., are printed and characterized using the near ideal outer-sphere redox probe hexaammineruthenium (III) chloride. The utilization of this probe has been chosen due to its outer-sphere redox mechanism that is insensitive to the C/O ratio groups and is affected only by the electronic structure of the 3D printed electrode (i.e., the origin of electrochemical activity, edge plane like-sites and defects); this is a commonly used redox probe in academic literature. Figure 2C shows the response of the electrode toward the near ideal outersphere ruthenium probes, which demonstrates that the addition of PVA into the polymer matrix initially worsens the performance of the electrode when compared to the 80% ABS and 20% Super P control, with a peak-to-peak separation of 78 and 68 mV respectively; this indicates a diffusional electrochemical (quasi-electrochemically reversible) response, as is seen for general electrode surfaces. Once the 80% ABS/PVA [1:1] and 20% Super P nanocarbon has been sonicated and the micropores exposed, the peak-to-peak separation becomes 47 mV, which clearly indicates thin-layer diffusional electrochemical activity, i.e., there is a clear evidence of microporosity within the electrode structure. This is confirmed with SEM of the surface as shown in Figure 2C. Interestingly, once the micropores have been introduced into the structure, the voltammetric responses exhibit sigmoidal behavior, especially at lower scan rates, however without the sonication of the AM/3D printed electrodes demonstrates a quasi-reversible electrochemical response. In summary, it is apparent that the AM/3D printed electrode demonstrates a larger increase in current handling capabilities and significantly improved electrochemical response with the introduction of micropores integrated into its structure.

Given the improved performance of the microporous electrodes, as shown above, this was then used as the basis for the development of the electrodes in the AM/3D printed cell utilized as the Na-ion battery. The AM/3D printed cells were assembled as shown within Figure 1, with $NaMnO_2$ integrated into the cathode and additionally TiO_2 integrated into the anode, both of which were manufactured with ABS/PVA [1:1] to improve the electrochemical activity. For comparative purposes, an ink-based battery within an AM/3D AM cell was developed (see Experimental Section), which is commonly used in the battery field. It is important to note that in the case of the ink-based battery, a separator was required in order to prevent any shorting between the electrodes, however in the case of the fully AM/3D printed structure, the cell's design allows for the electrolyte to be inserted without the need of any separator. In this case, the electrolyte is completely contained within the cell structure and the electrodes are held apart mechanically by the cell's design. Additionally, it is important to highlight that this approach means that the electrodes no longer require any current carriers, significantly reducing the manufacturing costs of the device as well as removing and required consideration to the interfacial, thin film, or constriction resistances that can negatively affect the performance of the battery.

Both cell types were cycled, charged and discharged under symmetric conditions, galvanostatically between +0.6 and +1.8 V within an ionic liquid electrolyte; **Figure 3** depicts the charge characteristics of the fully AM/3D printed approach, which can be directly compared to the ink based battery, as presented within Figure S5 (Supporting Information) under the same charging conditions. In both cases, the batteries demonstrate impressive charging characteristics, with gradual transitions. A significant potential increase in the low capacities for each cycles is observed, transitioning quickly from +0.6 V to approximately +1.4 V in the initial charge for both the ink-based battery with the AM/3D approach and the fully AM/3D printed system. Further to this, there are notable and obvious inconsistencies and fluctuations in the gradient through the charging and discharging, likely to be related to localized high points of resistance. There are a couple of potential causes for such fluctuation; first the relatively higher resistance of the electrodes, which consist of high polymer quantities can introduce instabilities in the charging characteristics, varying the internal resistance of the device, also, the electrical conductivity of the ionic electrolyte and the ionic behavior of the salt vary greatly with temperature and potential. Furthermore there is a gradual decline in the specific capacitance with cycling, starting at 84.3 mAh g^{-1} decreasing down to 11.1 mAh g^{-1}. This is likely to be attributed to the formation and uncontrolled build-up of the solid electrolyte interface (SEI) that is commonly observed in sodium-ion batteries, especially in with the utilization of sodium hexafluorophosphate ($NaPF_6$) and sodium tetrafluoroborate ($NaBF_4$).[27] The conductivities of ionic liquids electrolytes have been shown to greatly increase with increasing temperature, mainly because high temperatures can promote the dissolution of sodium salt $NaBF_4$, the creation of free ions and the increase in the migration rate of the effective carriers. However, with the

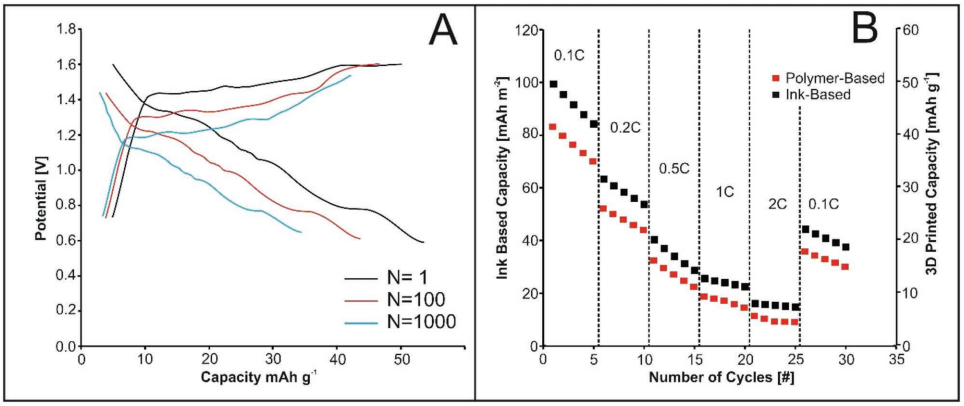

Figure 3. The energy storage characteristics of the AM/3D printed energy storage architectures: A) the polymer-based fully AM/3D printed structure for increasing number of cycles (N); B) the current impact on the galvanostatic charge discharge capacity.

addition of the $NaBF_4$ the conductivity of the electrolyte is lower than that of pure $EMIBF_4$, due to the increase in the electrolyte viscosity, which hinders the migration of Na^+.[28–31] In both cases, there is a close to typical response to the increase of the applied current. The increase of charging/discharging current is shown to significantly influence the performance, as typical with batteries under these test conditions.

Although this might be considered by some, generally by battery scientists, as not being such a ground-breaking performance, the mere fact that a device mostly constructed from thermoplastics, printed from a commercially available AM/3D printer, and demonstrates not only energy storage, but also the typical characteristics of batteries developed under clean room conditions is remarkable. The results here show the significant potential of AM/3D printing in the design and prototyping of energy storage concept in the third dimension. For a critical comparison, an ink-based approach was also considered where the cell was printed by AM/3D printing.

2. Conclusions

For the first time, a freestanding sodium-ion (full cell) battery formed entirely of components that have been fabricated via AM/3D printing, integrating active materials $NaMnO_2$ and TiO_2 within a porous supporting material, before being printed into a proof-of-concept model based upon the basic geometry of a commercially available AA battery, is reported. The AM/3D printed devices demonstrate a respectable performance of 84.3 mAh g^{-1} and are directly compared with a device that has been fabricated via a more typical manufacturing method utilizing an ink-based Na-ion battery within a AM/3D AM cell, which exhibited a specific capacity of 98.9 mAh m^{-2} (116.35 mAh g^{-1}). The relatively close comparison of the battery performance of this novel approach, i.e., a freestanding sodium-ion (full cell) battery formed entirely of components that have been fabricated via AM/3D printing which is composed of 80% plastic compared to a traditional ink-based approach, indicates that the AM/3D printing of batteries is clearly as way forward. Note that the reader must consider that these structures are typically made of 80% thermoplastic, and yet still work as a fully functioning energy storage platform and allow for batteries to be AM/3D printed into structures that are no-longer limited by traditional batteries. This represents a significant paradigm shift in the considerations of energy storage and battery design, providing a significant platform for the integration of a broad range of materials and architectures, to develop the next generation of energy storage architectures.

3. Experimental Section

All chemicals used were of an analytical grade and used without any further purification from Sigma-Aldrich unless stated otherwise. The solutions were prepared with deionized water of resistivity not less than 18 MΩ cm. Electrochemical measurements were carried out at room temperature using an Autolab PGSTAT302N (UK).

The $NaMnO_2$ was prepared by a solid-state synthesis adapted from Billaud et al.[20] The solid-state route involved mixing stoichiometric amounts of Na_2CO_3 and Mn_2O_3; with a 15% excess of the sodium to account for Na_2O evaporation upon firing. The mixing was carried out in a ball-mill using 10 mm diameter AlO_3 balls, with a ball-to-sample weight ratio of 30:1, at a milling speed of 450 rpm. The powder was then heat treated at 950° for 10 h with ramp speeds of 5.0 °C min^{-1}. The resulting material was stored under vacuum until used.

Powder XRD was performed on an X'pert powder PANalytical" model with a copper source of Kα radiation (of 1.54 Å) and Kβ radiation (of 1.39 Å), using a thin sheet of nickel with an absorption edge of 1.49 Å to absorb Kβ radiation. A reflection transmission spinner stage (15 rpm) was implemented to hold the commercially sourced $NaMnO_2$ powder. The range was set between 10° and 120° 2θ in correspondence with literature ranges.

Solid-state NMR experiments were performed under 60 kHz MAS, using a 1.3 mm double resonance HX probe. ^{23}Na 1D spin echo spectra were recorded at room temperature on a Bruker 400 MHz Avance III spectrometer (Germany) equipped with a triple resonance probe with the x-coil on the outside (TXO) flow probe that was linked directly to an automated SABRE polarization system.

All 3D printing composite filaments were prepared using a Thermo Haake Rheomix 600 mixing bowl fitted to a Thermo Haake Polydrive dynamometer unit. The bowl was fitted with Banbury rotors. All polymer-based composites were performed at 180 °C and at 70 rpm, utilizing a commercially available ABS [Axion ABS52 1003, Axion Group, UK]. In order to maximize the surface area of the electrodes a polymer microporous structure is utilized by mixing the composite with a PVA additive [M_w = 89 000–98000, Sigma], which is immiscible in the

ABS polymer, which can then be easily washed away by sonicating in water, leaving small pockets of vacancies in the polymer matrix. The polymer-based composites were granulated and extruded into a 3D printable filament of nominal thickness 1.85 mm, using a Thermo Fisher TSE 24 MC Twin-screw Extruder. All ink-based composites were mixed manually using a polymeric screen-printing ink binder for phosphor inks, from Gwent [Product number: R2131203D10, Gwent Electronic Materials Ltd, UK].

The 3D printed designs were drawn using 3DS's Solidworks and were printed utilizing either a FDM 3D printer (ZMorph, Warsaw, Poland), using a custom drilled 1.0 mm diameter nozzle to prevent blockages, or a stereolithography (SLA) printer (Form2, Formlabs, USA). Several designs were drawn, first a housing for 2D printed electrodes, which was printed using the SLA method to ensure the chassis was watertight to prevent any leakages or oxidization of the components. Second a pair of electrodes and a cell in the dimensions of a commonly used AA battery as a proof of concept of the application of 3D printing energy storage architectures. These designs are shown in Figure 1.

Ink Based Na-Ion Battery within an AM/3D AM Cell: The integration of active materials into a screen-printable formation was considered. The $NaMnO_2$ was mixed with Super P nanocarbon, in order to provide improved conductivity, and combined with a screen-printing ink binder from Gwent; this is known as the ink. A typical cell was AM/3D printed by a commercially available SLA 3D printer. First, the proof-of-concept ink based battery was constructed, consisting of a $NaMnO_2$ (64%), Super P nanocarbon (16%) and binder (20%) cathode, a TiO_2 nanopowder (64%), Super P nanocarbon (16%) and binder (20%) anode, consisting of 10 cm^2 electrodes mounted inside the 3D printed chassis and separator soaked in an electrolyte. Both electrodes were doctor bladed onto a 9 µm copper film [99.99% purity, MTI Corporation, USA], with a thickness of 10 µm. In order to ensure that any faults in the AM/3D printed cell did not cause any risk or dangerous properties during testing a highly stable and safe ionic liquid was utilized as an electrolyte. 1-Ethyl-3-methylimidazolium-bis-tetrafluoroborate ($EMIBF_4$) with an additive of sodium salt, namely sodium tetrafluoroborate, $NaBF_4$ has been show to demonstrate relative good performance, with high levels of environmental and thermal stability.[32,33] As such, an electrolyte of 0.5 M $NaBF_4$ in $EMIBF_4$ was utilized, with a cellulose separator. The chassis and lid were designed to fit tightly with a locking seal, to press the electrodes tightly together without leaking any electrolyte from the cell. Kapton tape was applied around the seals to ensure no leaking or loss of electrolyte. Figure S6 (Supporting Information) shows a photograph of an example of one of the completed cells.

Supporting Information

Supporting Information is available from the Wiley Online Library or from the author.

Acknowledgements

C.E.B. conceived the concept. M.D. designed the experiments. M.D., E.M.P., and C.W.F. undertook the experiments. C.E.B., M.D., and C.W.F. performed data analysis. All authors wrote the manuscript, and all the authors discussed the results, contributed to the draft of the manuscript, and commented on the final version. C.E.B. coordinated the overall project. Funding from the Engineering and Physical Sciences Research Council (Reference: EP/N001877/1). The Manchester Fuel Cell Innovation Centre is funded by the European Regional Development Fund.

Conflict of Interest

The authors declare no conflict of interest.

Keywords

3D printing, additive manufacturing, advanced materials, batteries, energy

Received: September 28, 2018
Revised: November 30, 2018
Published online: February 10, 2019

[1] Y. Zhang, C. W. Foster, C. E. Banks, L. Shao, H. Hou, G. Zou, J. Chen, Z. Huang, X. Ji, *Adv. Mater.* **2016**, *28*, 9391.
[2] J.-Y. Hwang, S.-T. Myung, Y.-K. Sun, *Chem. Soc. Rev.* **2017**, *46*, 3529.
[3] H. Hou, C. E. Banks, M. Jing, Y. Zhang, X. Ji, *Adv. Mater.* **2015**, *27*, 7861.
[4] H. Hou, L. Shao, Y. Zhang, G. Zou, J. Chen, X. Ji, *Adv. Sci.* **2017**, *4*, https://doi.org/10.1002/advs.201770002.
[5] S. W. Kim, D. H. Seo, X. Ma, G. Ceder, K. Kang, *Adv. Energy Mater.* **2012**, *2*, 710.
[6] B. L. Ellis, L. F. Nazar, *Curr. Opin. Solid State Mater. Sci.* **2012**, *16*, 168.
[7] V. Palomares, P. Serras, I. Villaluenga, K. B. Hueso, J. Carretero-Gonzalez, T. Rojo, *Energy Environ. Sci.* **2012**, *5*, 5884.
[8] G. Pang, P. Nie, C. Yuan, L. Shen, X. Zhang, J. Zhu, B. Ding, *Energy Technol.* **2014**, *2*, 705.
[9] W. Song, X. Ji, Z. Wu, Y. Zhu, Y. Yang, J. Chen, M. Jing, F. Li, C. E. Banks, *J. Mater. Chem. A* **2014**, *2*, 5358.
[10] T. Nagaura, K. Tozawa, *Prog. Batteries Sol. Cells* **1990**, *9*, 209.
[11] Z. Lu, D. D. MacNeil, J. R. Dahn, *Electrochem. Solid-State Lett.* **2001**, *4*, A191.
[12] A. Ambrosi, M. Pumera, *Chem. Soc. Rev.* **2016**, *45*, 2740.
[13] K. Sun, T.-S. Wei, B. Y. Ahn, J. Y. Seo, S. J. Dillon, J. A. Lewis, *Adv. Mater.* **2013**, *25*, 4539.
[14] E. García-Tuñon, S. Barg, J. Franco, R. Bell, S. Eslava, E. D'Elia, R. C. Maher, F. Guitian, E. Saiz, *Adv. Mater.* **2015**, *27*, 1688.
[15] C. Huber, C. Abert, F. Bruckner, M. Groenefeld, S. Schuschnigg, I., Teliban, C. Vogler, G. Wautischer, R. Windl, D. Suess, *Sci. Rep.* **2017**, *7*, 9419.
[16] N. Guo, M. C. Leu, *Front. Mech. Eng.* **2013**, *8*, 215.
[17] K. Fu, Y. Wang, C. Yan, Y. Yao, Y. Chen, J. Dai, S. Lacey, Y. Wang, J. Wan, T. Li, Z. Wang, Y. Xu, L. Hu, *Adv. Mater.* **2016**, *28*, 2587.
[18] C. W. Foster, M. P. Down, Y. Zhang, X. Ji, S. J. Rowley-Neale, G. C. Smith, P. J. Kelly, C. E. Banks, *Sci. Rep.* **2017**, *7*, 42233.
[19] X. Wei, D. Li, W. Jiang, Z. Gu, X. Wang, Z. Zhang, Z. Sun, *Sci. Rep.* **2015**, *5*, 11181.
[20] J. Billaud, R. J. Clément, A. R. Armstrong, J. Canales-Vázquez, P. Rozier, C. P. Grey, P. G. Bruce, *J. Am. Chem. Soc.* **2014**, *136*, 17243.
[21] T. Ma, G.-L. Xu, Y. Li, B. Song, X. Zeng, C. Sun, Y. Ren, S. M. Heald, J. Jorne, R. Shahbazian-Yassar, K. Amine, Z. Chen, in *Meeting Abstracts MA2016-02*, Honolulu, Hawaii, October **2016**, p. 667.
[22] X. Ma, H. , Chen, G. Ceder, *J. Electrochem. Soc.* **2011**, *158*, A1307.
[23] G. R. Zhang, L. J. Zou, Z. Zeng, H. Q. Lin, *J. Appl. Phys.* **2009**, *105*, 07E512.
[24] B. Fuchs, S. Kemmler-Sack, *Solid State Ionics* **1994**, *68*, 279.
[25] A. Mendiboure, C., Delmas, P. Hagenmuller, *J. Solid State Chem.* **1985**, *57*, 323.
[26] P. Suresh, A. K., Shukla, N. Munichandraiah, *J. Power Sources* **2006**, *161*, 1307.
[27] F. A. Soto, A. Marzouk, F. El-Mellouhi, P. B. Balbuena, *Chem. Mater.* **2018**, *30*, 3315.

[28] M. C. Buzzeo, R. G. Evans, R. G. Compton, *ChemPhysChem* **2004**, *5*, 1106.
[29] T. Y. Kim, H. W. Lee, M. Stoller, D. R. Dreyer, C. W. Bielawski, R. S. Ruoff, K. S. Suh, *ACS Nano* **2011**, *5*, 436.
[30] L. Mai, H. Li, Y. Zhao, L. Xu, X. Xu, Y. Luo, Z. Zhang, W. Ke, C. Niu, Q. Zhang, *Sci. Rep.* **2013**, *3*, 1718.
[31] M. Moreno, E. Simonetti, G. B. Appetecchi, M. Carewska, M. Montanino, G.-T. Kim, N. Loeffler, S. Passerini, *J. Electrochem. Soc.* **2017**, *164*, A6026.
[32] F. Wu, N. Zhu, Y. Bai, L. Liu, H. Zhou, C. Wu, *ACS Appl. Mater. Interfaces* **2016**, *8*, 21381.
[33] M. P. Down, C. E. Banks, *ACS Appl. Energy Mater.* **2018**, *1*, 891.

